INTERFEROMETRIC SEEING MEASUREMENTS AT LA SILLA

Claude Roddier and Francois Roddier
National Optical Astronomy Observatories*
Advanced Development Program
P.O. Box 26732, Tucson, AZ. 85726

1. INTRODUCTION

The transfer function for long-exposure astronomical images is the product of the telescope transfer function and the wavefront coherence function [1]. Since coherence is best measured interferometrically, interferometers appear to be the most appropriate tools to make accurate estimates of seeing quality, independent of the optical performance of the telescope. The advantages of interferometric measurements over other techniques were pointed out by Danjon as far back as 1955 [2]. In 1967, Coulman proposed an interferometric scheme to measure internal telescope seeing [3]. The first quantitative measurements on stars were obtained in 1973, independently by Roddier and Roddier [4] and by Kelsall [5] using point photoelectric detectors. Later, Dainty and Scaddan used a folding interferometer and an image intensifier to record the coherence function all at once [6,7]. Similar measurements were recently reported by O'Byrne [8]. Because fringes are concentrated in a small part of the telescope pupil, this method does not make use of all the photons available. In 1975, C. Roddier [9] used a rotational shear interferometer, optimizing the instrument efficiency by adjusting the angular shear to telescope size and seeing conditions. The increase in sensitivity was so large that it became possible to record fringes directly on Tri-X film without intensification. The instrument was later used simultaneously with a scidar to estimate the relative contribution of upper and lower layers in the atmosphere [10]. We describe here similar measurements made at La Silla during the February 1986 site testing campaign.

2. THE INSTRUMENT

The interferometer is schematically described in Fig. 1. It consists of a beam splitter cube S followed by two roof prisms A and B, one in each arm. We used a compact model specially designed and made at the optical shop of the Nice Observatory by Demarcq and Roussel. Birefringent quartz plates are attached in optical contact to each of the roof prisms for phase compensation as described by Roddier et al. [11]. The fixed roof prism with its quartz

*Operated by the Association of Universities for Rersearch in Astronomy, Inc., under contract with the National Science Foundation.

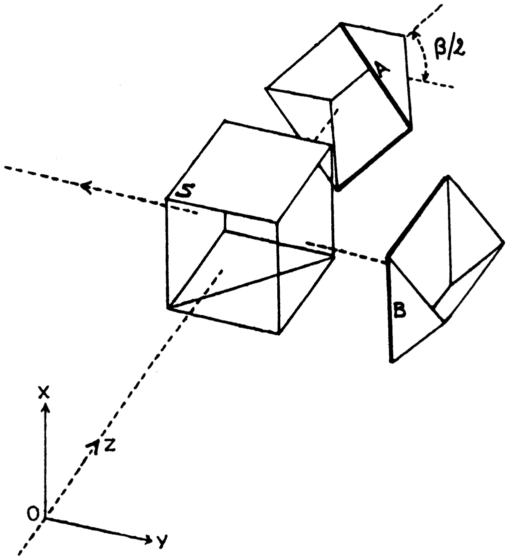

Figure 1: Sketch of the rotational shear interferometer.

plate is also attached in optical contact to one half of the beam splitter cube. The three remaining free parts are in contact with each other through an oil film, the thickness of which is determined by appropriate spacers. This configuration limits the necessary adjustments to four (two translations and two rotations) and is remarkably insensitive to mechanical vibrations. It also avoids stray light due to internal reflections. With a coherent point source the fringe visibility exceeds 95% at all rotation angles. A view of the interferometer and its mount is given in fig. 2.

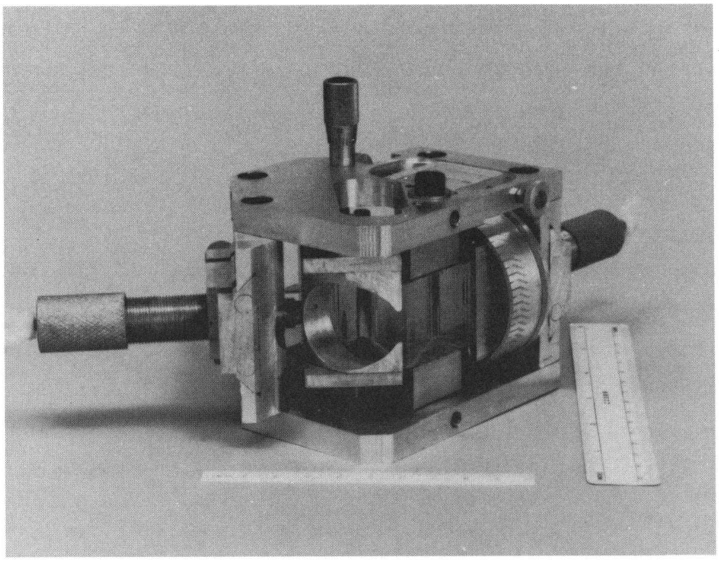

Figure 2: The interferometer in its mount.

Fig. 3 shows the instrument mounted on the ESO 50 cm telescope. First a folding mirror (A) centered in the telescope focal plane reflects light at a right angle along the flange on which the instrument is mounted. This mirror

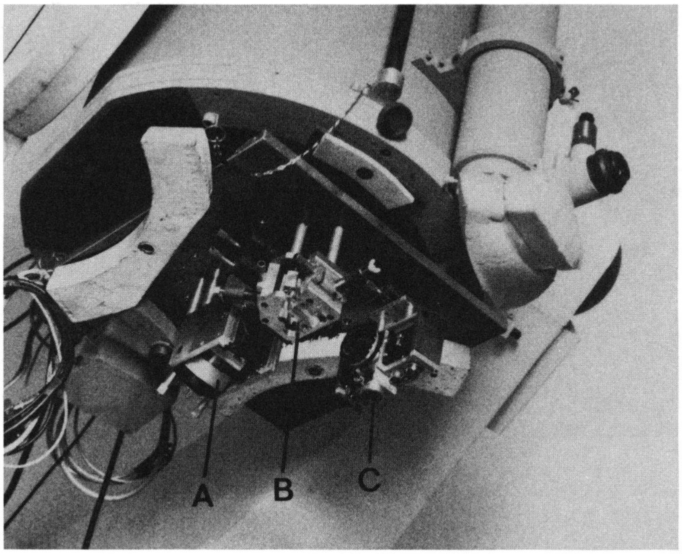

Figure 3: The instrument mounted on the ESO 50cm telescope.

is used to line up the telescope optical axis with the interferometer axis. An achromat then converts the diverging beam into a parallel beam and images the telescope pupil through the interferometer (B) onto the edges of the roof prisms. The interferometer produces two images of the pupil which exactly coincide when the axes are lined up. One roof prism can rotate about the optical axis, which makes the associated image rotate twice as fast producing an angular shear between the two images. A lens and a camera (C) are used to record on film the two superimposed pupil images on which interference fringes are observed. The size of the recorded image is about 4 mm. The fringe spacing can easily be adjusted either by tilting a prism or by changing the telescope pointing. Typically 30 fringes are recorded across the pupil. The shear angle is adjusted so that recorded fringes tend to disappear at the edge of the pupil.

Fringes were recorded on Tri-X film using bright stars near the zenith, in the following order: Alpha Canis Majoris (Sirius), Alpha Hydrae, and Beta Crucis. On Sirius we used a 90 Å bandwidth interference filter centered at 5340 Å, producing narrow-band fringes all over the telescope pupil. Fig. 4 shows such fringes recorded with two different angular shears. Frames with zero shear were also recorded for calibration. On the other stars, we recorded white light or broad-band fringes yielding information only in the direction of

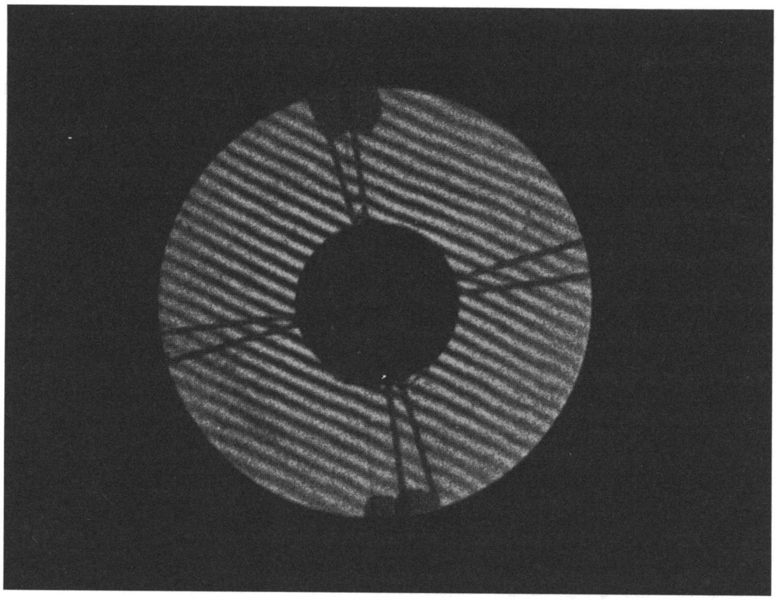

(a)

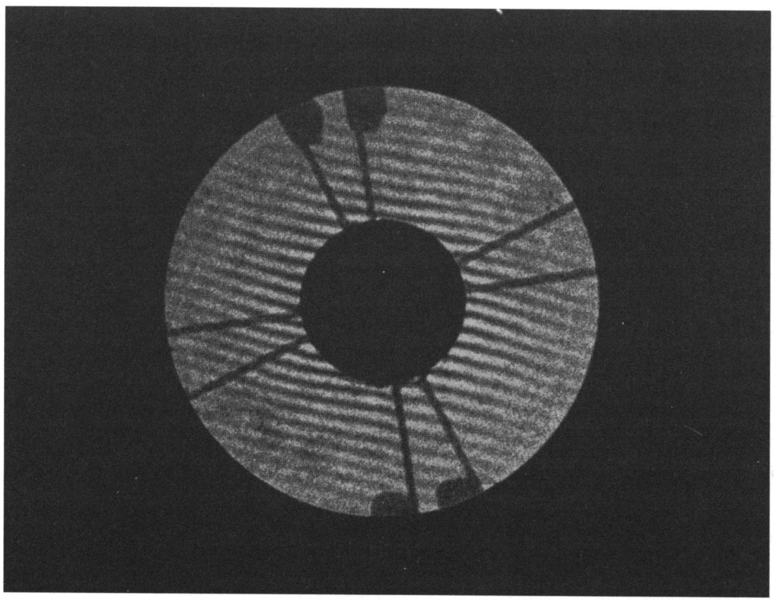

(b)

Figure 4: Examples of narrow-band interferograms recorded on Sirius. The shear angle is (a) 9°, (b) 18°.

their maximum extent. Typical exposure times ranged from a few tens of seconds to a few minutes, the longest exposures being limited by the telescope drive accuracy. For each shear angle, frames without fringes were recorded in order to make corrections for non-uniformities of the continuum. Films were photometrically calibrated.

3. DATA REDUCTION

The data consist of a set of 44 films of 20 exposures each i.e., a total of 880 frames. Clearly, direct recording and digitization of the interferograms with a CCD camera would have been preferable. However, we did not initially intend to process all the data. We intended to use only some of them to calibrate the differential image motion monitor built by ESO. Because this instrument was not yet fully operational at the time of the campaign, it was later decided to analyze the full set.

The narrow-band interferograms taken on Sirius were digitized over 256 x 256 sample points with a PDS microdensitometer. Density levels were converted into illumination levels using the film calibration. Once digitized, frames were viewed through an image processing system (IRAF at NOAO) and geometrical measurements were made to locate the pupil edges and the spider arms. Each file was then processed interactively on a VAX computer. A new improved algorithm was used to map the fringe visibility over each interferogram [12]. First the algorithm corrects the fluctuations of the continuum due to imperfections in the optics, using frames recorded without fringes. Fig. 5

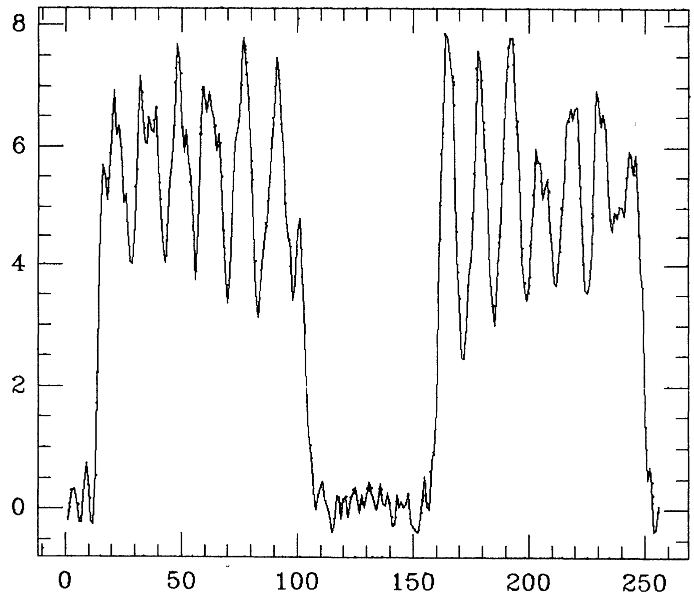

(a)

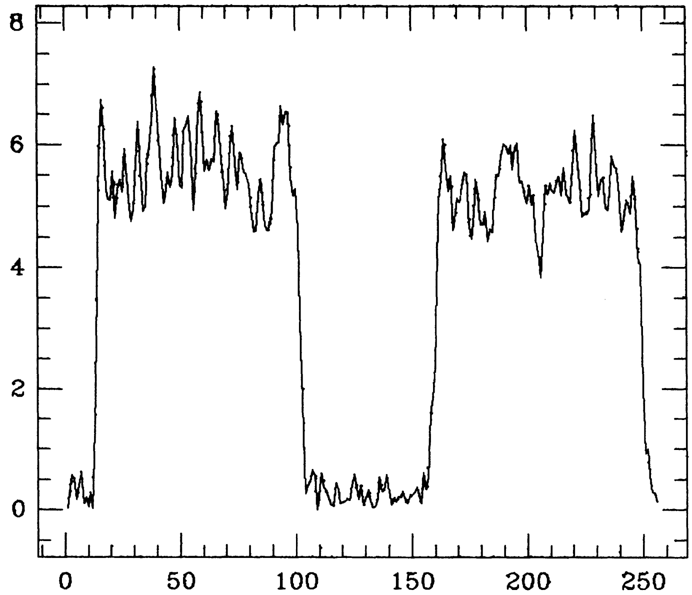

(b)

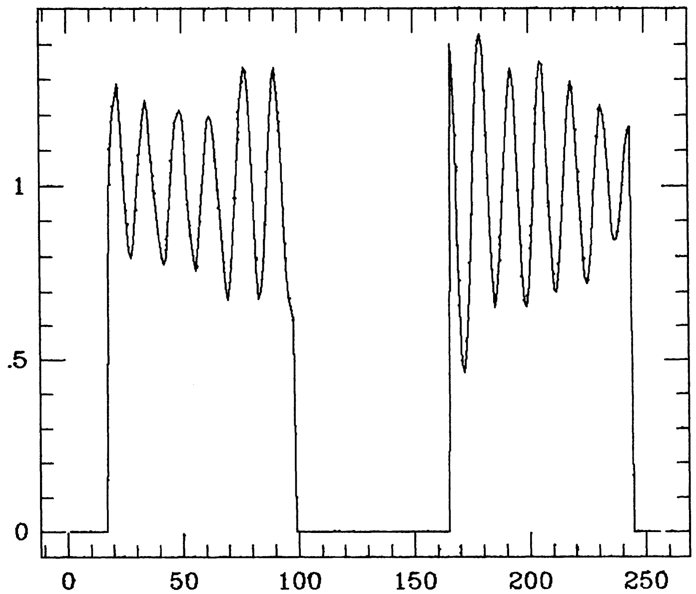

(c)

Figure 5: Example of correction for the fluctuations of the continuum. a) raw data, b) estimated continuum, c) corrected data.

shows an example of such a correction. Fig. 5a shows the raw data, fig. 5b shows the estimated continuum, and fig. 5c shows the corrected data. Based on a systematic use of two-dimensional Fourier transforms, the algorithm filters out most of the noise. It also interpolates and/or extrapolates the signal, minimizing the error at the interferogram boundaries.

The fringe visibility was averaged over concentric circles after elimination of the lowest values, believed to be produced by imperfections in the optics or possible local seeing effects inside the telescope. The resulting visibility estimate V(r), as a function of the baseline r, was then compared to the theoretical law

$$V(r) = V(0)\ \exp\left(-3.44(r/r_o)^{5/3}\right) \tag{1}$$

Plots of log $\left(\log V(r)\right)$ as a function of log r were made together with a least-squares fit with a straight line. In most cases the slope was found to agree with the 5/3 law within 10%, often much better. Fried's parameter r_o was obtained from least square fits with a 5/3 slope. Fig. 6 shows such plots. On a few occasions departures from Kolmogorov's law were observed, showing evidence for incompletely developed turbulence, in which case r_o becomes ill-defined.

The wide-band interferograms were reduced using a simplified procedure. Each frame was scanned with a slit parallel to the fringes, producing 42 lines with 256 samples per line. Local least-squares fits with a sine function were used to estimate the fringe visibility, keeping only the maximum value observed on each line. Comparison with the theoretical law of Eq. (1) was made as described above.

Once estimates of r_o were obtained for each frame, wavelength corrections were made to derive values of r_o at $\lambda = 0.5$ µm according to the scaling law $r_o \propto \lambda^{5/6}$. For wide-band observations, the scaling factor was chosen so as to get the best agreement with narrow-band measurements made nearly at the same time. Further corrections were made to derive values of r_o at zenith angle z = 0 using the scaling law $r_o \propto (\cos z)^{3/5}$. The full width half maximum seeing angle was taken as $\alpha = 0.98\lambda/r_o$, assuming $\lambda = 0.5$ µm. For each observation the integrated value of the refractive index structure coefficient C_N^2 was also derived using the relationship

$$\int_0^{\infty} C_N^2(h)dh = 6.83\cdot 10^{-13}\ \alpha^{5/3} \tag{2}$$

where α is measured in arc-seconds and the integral of C_N^2 is in $m^{1/3}$. This is to be compared with the sum of the contributions of the different atmospheric layers derived from measurements made with other sensors such as the sodar (for ground turbulence) and the scidar (for free air turbulence).

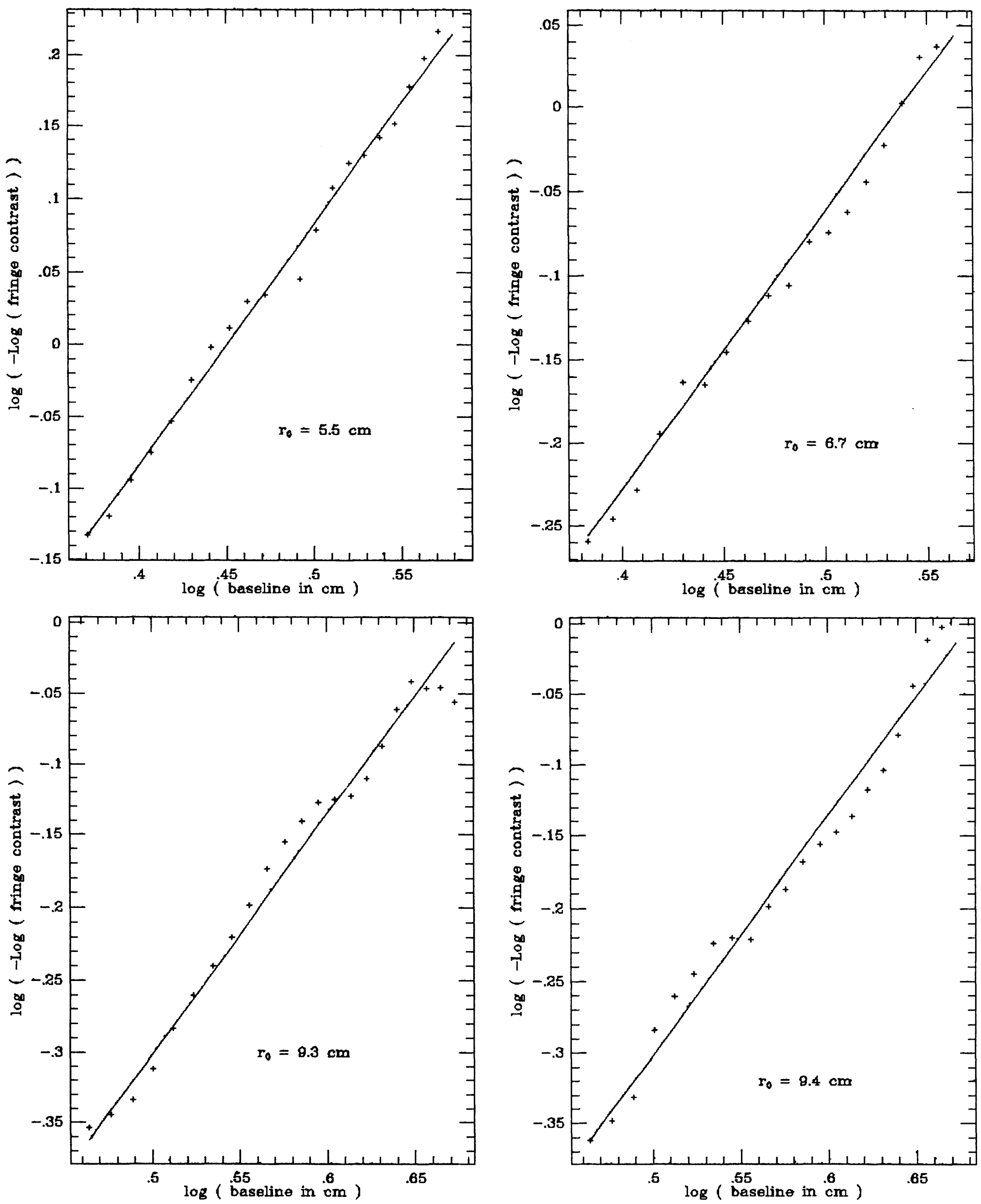

Figure 6: Examples of plots of the log of the log visibility as a function of the log baseline and best fit with a 5/3 slope.

4. FIRST RESULTS

Circles on fig. 7 show the result of the seeing measurements made during the night of Feb. 14th. Crosses plotted on the same figure show the seeing estimated by adding the contributions measured by the sodar and the scidar.

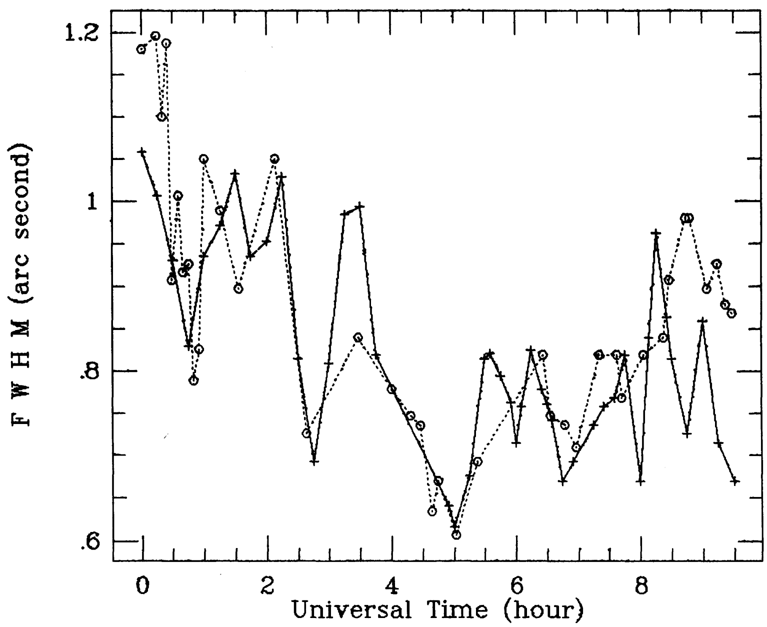

Figure 7: Results of seeing measurements made during the night of February 14 (circles). Crosses indicate the seeing estimated by adding the contribution measured by the sodar and the scidar.

The contribution of free air turbulence measured by the scidar was only about 10%. Because uncertainty remains in the sodar calibration, a factor 0.67 was applied to the sodar contribution in order to get the best fit around 5:00 U.T.. Clearly the two estimates correlate very well.

Acknowledgement

The reduction of the 880 interferograms was made possible with the help of a summer student, Nick Strobel, supported on ESO funds.

References

[1] F. Roddier, Progress in Optics, **19**, (1981) 281.
[2] A. Danjon, Vistas Astron., **1**, (1955) 377.
[3] C.E. Coulman, Proc. ASA, **1**, (1967) 67.
[4] C. Roddier and F. Roddier, J. Opt. Soc. Am., **63**, (1973) 661.
[5] D. Kelsall, J. Opt. Soc. Am., **63**, (1973) 1472.
[6] J.C. Dainty and R.J. Scaddan, Mon. Not. R. astr. Soc., **167**, (1974) 69P.
[7] J.C. Dainty and R.J. Scaddan, Mon. Not. R. astr. Soc., **170**, (1975) 519.
[8] J.W. O'Byrne, Proc. ASA, **6**, (1985) 43.
[9] C. Roddier, J. Opt. Soc. Am., **66**, (1976) 478.
[10] C. Roddier and J. Vernin, Appl. Opt., **16**, (1977) 2252.
[11] F. Roddier, C. Roddier and J. Demarcq, J. Optics (Paris), **9**, (1978) 145.
[12] C. Roddier and F. Roddier, "Interferogram analysis using Fourier-transform techniques", submitted to Applied Optics.

DISCUSSION

E.J. Wampler: If dome seeing is important then the turbulence in the dome is significant. Do your theories tell how much the image is degraded if the Cassegrain focus is used (3x through the atmosphere) rather than the prime focus (2x through the atmosphere)?

C. Roddier: This can be calculated if we can model the distribution of turbulence in the telescope (uniform?) and its spectrum (Kolmogorov?). Clearly, the degradation will increase with the path length, but narrow beams are much less degraded than large beams so that the difference between a Cassegrain focus and a prime focus may be small.